2015 IEEE International Conference on Robotics and Automation (ICRA)
Washington State Convention Center
Seattle, Washington, May 26-30, 2015

Point-to-Point Motion Control of a Unicycle Robot: Design, Implementation, and Validation*

Yusie Rizal†, Chun-Ting Ke†, and Ming-Tzu Ho†,§

Abstract— **This paper presents the design, implementation, and validation of balance control and point-to-point motion control of a single-wheeled (unicycle) robot. The robot consists of a wheel, a body, a reaction wheel, and a turntable. The wheel is used to move the robot forward and backward to obtain longitudinal stability. The reaction wheel is used for obtaining lateral stability. The turntable provides steering torque about the vertical axis of the robot. The dynamic model of the system is derived using Euler-Lagrange formulation. By retaining the predominant nonlinear terms and neglecting the high-order coupling terms, the system model is simplified to three decoupled systems. Sliding mode control is then used to design the balance and steering controllers for the simplified model. By combining the obtained balance control and steering control, a point-to-point motion control strategy is proposed. The experimental results are presented to verify the effectiveness of the designed control schemes.**

I. INTRODUCTION

On hard and even terrains, wheeled locomotion is the most commonly used locomotion mechanism in mobile robotics due to its simplicity, good energy efficiency, and high payload-weight-to-mechanism-weight ratio. Wheeled mobile robots usually have three or more wheels to provide static stability and sufficient traction. However, multi-wheeled robots require more wheel driving and a larger chassis than those for a single-wheeled robot. Wheel suspension systems are required for multi-wheeled robots to ensure that the wheels are in contact with the ground at all times. The main advantages [1,2] of a single-wheeled robot over a multi-wheeled robot are a larger margin of clearance when passing obstacles, better dynamic stability, and a lower space requirement. However, a single-wheeled robot has high nonlinearity, instability, and underactuation in both longitudinal and lateral directions. These make the control design of a single-wheeled robot a highly challenging task. Single-wheeled robots have various configurations with different types of driving wheel (conventional wheel [1,3–10], spherical wheel [2], rugby-ball-shaped wheel [11]), and various mechanisms for stabilization and control, including those based on control moment gyroscopes [1,7], reaction wheels [8,9], turntables [3–6,8], and lateral pendulums [10]. A unicycle robot [3–10] is a specific type of single-wheeled robot that has its body sitting on the shaft of the driving wheel. In the past few years, various approaches [3–10] have been proposed to balance and control unicycle robots.

In our previous work [12], problems related to the balance control of a unicycle were addressed. In that work, the unicycle robot consisted of a wheel, a body frame, and a reaction wheel. The wheel enables the robot to move forward or backward for longitudinal balancing, while the reaction wheel is used for lateral balancing. By retaining the predominant nonlinear terms and neglecting the high-order coupling terms, the longitudinal dynamics and lateral dynamics are simplified to two decoupled systems. Sliding mode control [13,14] was used to design a stabilizing controller for the decoupled longitudinal system, while stabilization of the decoupled lateral system was based on feedback linearization [15]. The present study adds a turntable on the top of the robot to provide steering ability. A detailed dynamic model of the system is derived. For control design purposes, the detailed dynamic model is far too complex. Using the decoupling method introduced in [9,12], the system model is simplified to decoupled longitudinal dynamics, lateral dynamics, and yaw dynamics. The high-order coupling terms of the dynamics are treated as unknown disturbances. Sliding mode control [13,14] is known to be a robust control technique appropriate for controlling uncertain systems. To enhance robustness to the uncertainty due to model simplification and to attenuate external disturbances, sliding mode control is then applied to design the stabilizing controllers for the decoupled longitudinal system and lateral system. Steering control of the robot actuated through the turntable is also based on the sliding mode control. Point-to-point motion control is achieved by a simple combination of position regulation control and steering control. The effectiveness of the designed controllers is validated through experimental studies.

The rest of this paper is organized as follows. In Section II, a brief description of the experimental setup is given. In Section III, the mathematical model of a unicycle robot is presented and the longitudinal, lateral, and yaw dynamics of the system are decoupled and simplified. The design of sliding mode controllers for stabilization and steering control is given in Section IV. The point-to-point motion control is given in Section V. In Section VI, the experimental results are presented. Finally, Section VII contains some concluding remarks.

II. SYSTEM DESCRIPTION

The experimental setup of the unicycle robot is shown in Fig. 1(a), and a schematic overview of the system is shown

*This work was supported by the Ministry of Science and Technology of Taiwan under grants NSC 101-2221-E-006-189 and MOST 103-2221-E-006-184.

†The authors are with Department of Engineering Science, National Cheng Kung University, 1 University Road, Taiwan.

§Corresponding author (e-mail: bruceho@mail.ncku.edu.tw).

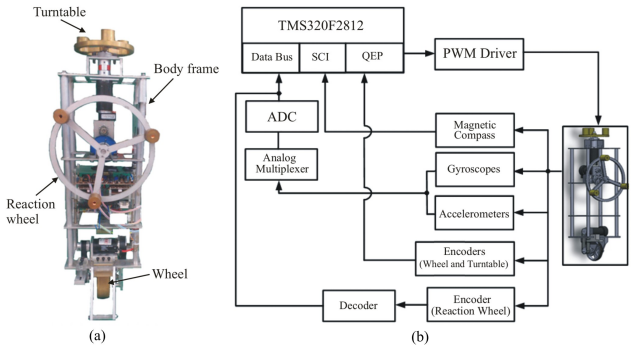

Fig. 1. Unicycle robot system: (a) front view of unicycle robot and (b) schematic diagram of experimental setup.

in Fig. 1(b). The robot consists of a wheel, a body frame, a reaction wheel, and a turntable. The wheel is driven by a dc motor via a timing belt. A dc motor with gear ratio of 3:1 is used to drive the reaction wheel. The turntable is directly coupled to a dc motor. The designed controllers are implemented on a digital signal processor (DSP) board in the C language. This DSP board is equipped with quadrature encoder pulse (QEP) units. The sampling frequency of the system is chosen to be 1 kHz. The angular displacements of the wheel, reaction wheel, and turntable are measured by optical encoders with a resolution of 2000 pulses/rev. The quadrature encoder signals generated by the optical encoders are connected to the QEP units on the DSP board. The angular velocities of the wheel, reaction wheel, and turntable are estimated from the displacement traveled per unit time and then passed through digital low-pass filters to attenuate the high-frequency noise. Three MEMS-based single-axis gyroscopes, two single-axis accelerometers, and a magnetic compass are used to obtain the attitude and orientation of the robot through a sensor fusion process. The pulse-width modulation (PWM) signals are generated according to the designed control laws and supplied to the PWM driver circuits that drive the dc motors.

III. SYSTEM MODELING

3.1 Model of the Unicycle Robot

The dynamic equations of the unicycle robot are derived using the Euler-Lagrange formulation [16]. The basic features of a unicycle robot are illustrated in Fig. 2 and the parameters of the system are given in Table I. Let *OXYZ* be the world frame and $ox_by_bz_b$ be the body fixed frame attached to the body of the robot with the origin coinciding with the center of the wheel, the z_b-axis is along the body of the robot, and y_b-axis is aligned with the rotation axis of the wheel. The Euler-Lagrange equation is

$$\frac{d}{dt}\left[\frac{\partial L}{\partial \dot{q}}\right] - \frac{\partial L}{\partial q} = Q, \tag{1}$$

where L is the Lagrangian function; Q and q are the generalized forces and generalized coordinates, respectively. The Lagrangian function L is defined as

$$L = T - V, \tag{2}$$

TABLE I
DEFINITIONS OF PARAMETERS OF SYSTEM

α	Pitch angle
β	Roll angle
γ	Yaw angle
θ, ϕ, ψ	Angular displacements of the wheel, reaction wheel, and turntable, respectively
m_w, m_b, m_d, m_f	Masses of the wheel, body, turntable, and reaction wheel, respectively
τ_w, τ_d, τ_f	Torques exerted on the wheel, reaction wheel, and turntable, respectively
I_{wx}, I_{wy}, I_{wz}	Moments of inertia of the wheel about the x_b, y_b, and z_b axes, respectively
I_{bx}, I_{by}, I_{bz}	Moments of inertia of the body about the x_b, y_b, and z_b axes, respectively
I_{dx}, I_{dy}, I_{dz}	Moments of inertia of the reaction wheel about the x_b, y_b and z_b axes, respectively
I_{fx}, I_{fy}, I_{fz}	Moments of inertia of the turntable about the x_b, y_b and z_b axes, respectively
l	Length from wheel to turntable
l_r	Radius of wheel
l_{wd}	Length from reaction wheel to turntable
(x, y)	Coordinates of contact point on the ground

where T is the kinetic energy and V is the potential energy. For this system, q is selected as

$$q = [\alpha \quad \beta \quad \gamma \quad \phi \quad \theta \quad \psi]^{\mathrm{T}}, \tag{3}$$

Q is given by

$$Q = [0 \quad 0 \quad 0 \quad \tau_d \quad \tau_w \quad \tau_f]^{\mathrm{T}}. \tag{4}$$

By computing (1), the dynamic equations of the unicycle system are obtained. The resulting dynamic equations of the system are far too lengthy to be shown here due to space limitation; hence, the reader is referred to another study [17]. The dynamics of this system are highly coupled and nonlinear. They are far too complex for control design purposes, so model simplification is necessary. It is assumed that the operating ranges of α and β are small. Instead of linearizing the nonlinear model with respect to its equilibrium, the predominant nonlinear terms of the system are retained, but the high-order coupling terms are neglected, as they are small. The dynamics of the system is decoupled and simplified to three parts: longitudinal, lateral, and yaw dynamics.

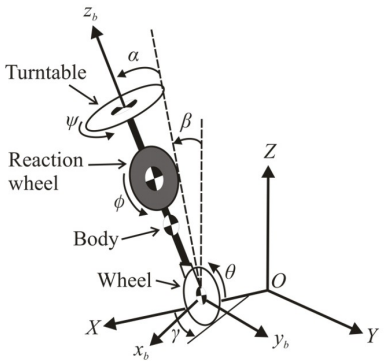

Fig. 2. Unicycle robot.

3.2 Simplification of System Dynamics

First, the longitudinal dynamics of the unicycle system is considered. Assuming that the roll angle and roll angular rate are small, the turntable and reaction wheel barely spin. By regarding the robot body, turntable, and reaction wheel as a single body, the longitudinal dynamics of the system can be simplified to a wheeled inverted pendulum system [18] as follows

$$\begin{aligned}&\left(I_{by}+I_{dy}+I_{fy}+\frac{l^2}{4}(m_b+4m_f)+l_{wd}^2m_d\right)\ddot{\alpha}\\&+\left(l_{wd}m_d+\frac{lm_b}{2}+lm_f\right)l_r\ddot{\theta}\cos\alpha\\&-\left(l_{wd}m_d+\frac{lm_b}{2}+lm_f\right)g\sin\alpha=0,\end{aligned}\tag{5}$$

$$\begin{aligned}&l_r\left(l_{wd}m_d+\frac{lm_b}{2}+lm_f\right)\ddot{\alpha}\cos\alpha\\&-ll_r(m_d+\frac{m_b}{2}+m_f)\dot{\alpha}^2\sin\alpha\\&+\left(I_{wy}+l_r^2(m_b+m_d+m_f+m_w)\right)\ddot{\theta}=\tau_w+d_w.\end{aligned}\tag{6}$$

where d_w is a disturbance torque representing the unmodeled dynamics due to model simplification and friction.

Assuming that the pitch angle and pitch angular rate are small, the turntable and wheel barely spin. By regarding the robot body, turntable, and wheel as a single body, the lateral dynamics of the system can be simplified to a reaction wheel inverted pendulum system [19] as follows

$$\begin{aligned}&I_{dx}\ddot{\phi}+\big((I_{bx}+I_{dx}+I_{fx}+I_{wx}+l_{wd}^2m_d+l^2m_f)\\&+\frac{m_b}{4}(l+2l_r)^2+2l_r(l_{wd}m_d+lm_f)\\&+l_r^2(m_d+m_f+m_w)\big)\ddot{\beta}-(l_r(m_d+m_f+m_w)\\&+\frac{m_b}{2}(l+2l_r)+l_{wd}m_d+lm_f)\,g\sin\beta=0,\end{aligned}\tag{7}$$

$$I_{dx}\ddot{\phi}+I_{dx}\ddot{\beta}=\tau_d+d_d,\tag{8}$$

where d_d is a disturbance torque representing the unmodeled dynamics due to model simplification and friction.

Assuming that the wheel and reaction wheel barely spin, about the upright position, the yaw dynamics of the system can be simplified to

$$I_{fz}\ddot{\psi}+(I_{wz}+I_{dz}+I_{bz}+I_{fz})\,\ddot{\gamma}=0,\tag{9}$$

$$I_{fz}\ddot{\psi}+I_{fz}\ddot{\gamma}=\tau_f+d_f.\tag{10}$$

where d_f is a disturbance torque representing the unmodeled dynamics due to model simplification and friction.

The dc motors are used to actuate the wheel, reaction wheel, and turntable. Since the electrical time constant of a dc motor is usually much smaller than the mechanical time constant, and the value of the viscous friction coefficient is negligible. The following reduced-order model of the dc motor is adopted

$$\tau_m=\frac{nK_t}{R_a}u-\frac{n^2K_t^2}{R_a}\omega_m,\tag{11}$$

where τ_m is the motor torque, n is the gear ratio, u is the control voltage, K_t is the motor torque constant, ω_m is the angular velocity of the motor, and R_a is the armature resistance. The physical parameters of the unicycle system can be founded in [17].

IV. CONTROLLER DESIGN

4.1 Balance Control Design

The first control problem is to balance the body of the robot in the upright position and regulate the rotational angle of the wheel such that the robot can move along a desired linear displacement in the longitudinal direction. Here, based on sliding mode control [13,14], the stabilizing controllers for the simplified longitudinal and lateral dynamics of the system are designed.

A. Stabilization of Longitudinal Dynamics

Let θ^* be the reference angle of the wheel. Then, e_θ is defined as the difference between the actual angle of the wheel and the reference angle of the wheel as follows

$$e_\theta=\theta-\theta^*.$$

From (5), (6), and (11), the dynamic equations are rewritten as follows

$$\begin{aligned}\ddot{\alpha}&=[HG_w\sin\alpha-N^2\dot{\alpha}^2\cos\alpha\sin\alpha+R_mK_tN\dot{e}_\theta\cos\alpha\\&\quad-R_mN\cos\alpha e_w]/[MH-N^2\cos^2\alpha],\end{aligned}\tag{12}$$

$$\begin{aligned}\ddot{e}_\theta&=[-NG_w\cos\alpha\sin\alpha+MN\dot{\alpha}^2\sin\alpha-MR_mK_t\dot{e}_\theta\\&\quad+MR_me_w+Md_w]/[MH-N^2\cos^2\alpha]\end{aligned}\tag{13}$$

where e_w is the control voltage, and

$$\begin{aligned}M&=m_dl_{wd}^2+\frac{1}{4}m_bl^2+m_fl^2+I_{dy}+I_{by}+I_{fy},\\N&=m_fll_r\cos\alpha+m_dl_{wd}l_r\cos\alpha+\frac{1}{2}m_bll_r\cos\alpha,\\H&=m_wl_r^2+m_dl_r^2+m_bl_r^2+m_fl_r^2+I_{wy},\\G_w&=\frac{1}{2}m_bgl+m_dgl_{wd}+m_fgl,\\R_m&=\frac{K_t}{R_a},\end{aligned}$$

and $MH-N^2\cos^2\alpha\neq0$.

To obtain the regular form [14,20], the following variable is used

$$y_s=e_\theta-\varphi(\alpha),\tag{14}$$

where $d\varphi(\alpha)/d\alpha=-M/(N\cos\alpha)$. It follows that

$$\varphi(\alpha)=\frac{M}{N}\ln\frac{1+\tan(\alpha/2)}{1-\tan(\alpha/2)}.\tag{15}$$

Then, the regular form of the system is given by

$$\ddot{y}_s=G_s(\alpha,\dot{\alpha})\tan\alpha\tag{16}$$

$$\ddot{\alpha}=v_s(\alpha,\dot{\alpha},\dot{e}_\theta,e_w)+d_1\tag{17}$$

where

$$G_s(\alpha,\dot{\alpha})=\frac{g}{l_r}+\frac{M}{N\cos\alpha}\dot{\alpha}^2,\tag{18}$$

$$\begin{aligned}v_s(\alpha,\dot{\alpha},\dot{e}_\theta,e_w)&=\left[HG_w\sin\alpha-N^2\dot{\alpha}^2\cos\alpha\sin\alpha\right.\\&\left.+R_mN\cos\alpha(K_t\dot{e}_\theta-e_w)\right]/\left[MH-N^2\cos^2\alpha\right],\end{aligned}\tag{19}$$

and

$$d_1 = -N\cos\alpha\ d_w/[MH - N^2\cos^2\alpha]. \tag{20}$$

The design of a sliding mode controller for locally stabilizing (18) and (19) in the presence of disturbance of (20) can be found in [12].

B. Stabilization of Lateral Dynamics

Since the angular displacement ϕ is a cyclic coordinate, it does not appear in the Lagrangian. Thus, this cyclic variable can be ignored in the equations of motion given in (7)-(8) and state variables $[z_1\ \ z_2\ \ z_3]^{\mathrm{T}} = [\beta\ \ \dot{\beta}\ \ \dot{\phi}]^{\mathrm{T}}$ can be defined to obtain the following reduced-order system

$$\begin{cases} \dot{z}_1 = z_2 \\ \dot{z}_2 = az_3 + b\sin z_1 + e\cdot e_d + e_1\cdot d_d \\ \dot{z}_3 = cz_3 + d\sin z_1 + f\cdot e_d + e_2\cdot d_d \end{cases} \tag{21}$$

where e_d is the control voltage, and

$$\begin{aligned} a &= \frac{n^2K_t^2}{R_a(M_\beta - I_{dx})}, \qquad b = \frac{N_\beta}{M_\beta - I_{dx}}, \\ c &= \frac{n^2K_t^2M_\beta}{R_aI_{dx}^2 - R_aI_{dx}M_\beta}, \quad d = \frac{N_\beta}{I_{dx} - M_\beta}, \\ e &= -\frac{nK_t}{R_a(M_\beta - I_{dx})}, \qquad f = -\frac{nK_tM_\beta}{R_aI_{dx}^2 - R_aI_{dx}M_\beta}, \\ e_1 &= -\frac{1}{(M_\beta - I_{dx})} \qquad e_2 = -\frac{M_\beta}{I_{dx}^2 - I_{dx}M_\beta} \\ M_\beta &= m_wl_r^2 + m_dl_r^2 + m_bl_r^2 + m_fl_r^2 + m_bll_r + 2m_fll_r \\ &\quad +2m_dl_{wd}l_r + m_fl^2 + m_dl_{wd}^2 + \frac{1}{4}m_bl^2 \\ &\quad +I_{bx} + I_{wx} + I_{dx} + I_{fx}, \text{and} \\ N_\beta &= m_fgl + \frac{1}{2}m_bgl + m_dgl_{wd} + m_fgl_r + m_dgl_r \\ &\quad +m_bgl_r + m_wgl_r. \end{aligned}$$

To obtain the regular form, a change of variables is used

$$y_\beta = z_2 - \frac{e}{f}z_3. \tag{22}$$

Differentiating (22) and substituting (21) into it yields the regular form of the system

$$\begin{aligned} \dot{y}_\beta &= A\sin z_1, \\ \dot{z}_1 &= z_2, \\ \dot{z}_2 &= v + d_2. \end{aligned} \tag{23}$$

where

$$A = \frac{(bf - ed)}{f}, \tag{24}$$

$$v = az_3 + b\sin z_1 + e\cdot e_d, \tag{25}$$

and

$$d_2 = e_1\cdot d_d. \tag{26}$$

Note that for this system $A > 0$. It follows that

$$e_d = \frac{1}{e}[v - az_3 - b\sin z_1]. \tag{27}$$

The following sliding manifold is chosen

$$s_\beta = \dot{s}_{1\beta} + \delta_\beta s_{1\beta} = 0, \tag{28}$$

where $\delta_\beta > 0$ and

$$s_{1\beta} = A\sin z_1 + \delta_{1\beta}\, y_\beta \tag{29}$$

with $\delta_{1\beta} > 0$. From (29), in the sliding manifold $s_\beta = 0$, which gives $s_{1\beta} \to 0$ as $t \to \infty$. This yields $A\sin z_1 = -\delta_{1\beta}\, y_\beta$ as $t \to \infty$. From (23), it follows that

$$\dot{y}_\beta = -\delta_{1\beta}\, y_\beta. \tag{30}$$

It is clear that (30) is asymptotically stable since $y_\beta \to 0$ as $t \to \infty$. It follows that $z_1 \to 0$ and $\dot{s}_{1\beta} \to 0$ as $t \to \infty$. From (29), one can obtain

$$\dot{s}_{1\beta} = A\dot{z}_1\cos z_1 + \delta_{1\beta}\,\dot{y}_\beta. \tag{31}$$

From $\dot{y}_\beta \to 0$, $\dot{s}_{1\beta} \to 0$, $\dot{z}_1 = z_2$, and (31), it follows that $z_2 \to 0$ as $t \to \infty$. Consequently, from (22), $z_3 \to 0$ as $t \to \infty$. This proves that in the sliding manifold, the system converges to its equilibrium.

By differentiating both sides in (28) and from (29), one can obtain

$$\dot{s}_\beta = A\,v\,\cos z_1 + A\,d_2\,\cos z_1 + F_\beta(\dot{z}_1, z_1), \tag{32}$$

where

$$\begin{aligned} F_\beta(\dot{z}_1, z_1) = &-A(\dot{z}_1)^2\sin z_1 + \delta_{1\beta}\,A\,\dot{z}_1\cos z_1 \\ &+\delta_\beta\,(A\dot{z}_1\cos z_1 + \delta_{1\beta}\,A\,\sin z_1)\,. \end{aligned} \tag{33}$$

It is assumed that d_2 is bounded and $|d_2| \le \bar{d}_2$, where $\bar{d}_2$ is a known constant. In order to ensure that the system reaches the sliding manifold s_β for any initial condition and that the sliding mode exists on s_β, the following is chosen

$$v = \frac{1}{A\cos z_1}\left[-V_{0\beta}\,\mathrm{sgn}(s_\beta) - F(\dot{z}_1, z_1)\right], \tag{34}$$

with $V_{0\beta} > A\bar{d}_2$ and $|z_1| < \pm\frac{\pi}{2}$ such that the reachability condition [13,14] of

$$\dot{s}_\beta s_\beta \le -\eta|s_\beta| \tag{35}$$

is satisfied with $\eta > 0$. Finally, from (27) and (34), the control voltage is given by

$$\begin{aligned} e_d = \frac{1}{e}\{&\frac{1}{A\cos z_1}[-V_{0\beta}\,\mathrm{sgn}(s_\beta) - F_\beta(z_1, z_2)] \\ &-az_3 - b\sin z_1\}. \end{aligned} \tag{36}$$

In order to eliminate the chattering problem [13,14], the $\mathrm{sgn}(\cdot)$ term in the control law is replaced by a saturation function [21]. This yields the motion of the system in a boundary layer of the sliding manifold instead of on the manifold.

4.2 Steering Angle Control of Yaw Dynamics

To control the orientation angle of the robot, a steering controller for the yaw dynamics is designed based on sliding mode control. e_γ is defined as the difference between the yaw angle of the robot and the reference yaw angle γ^* as follows

$$e_\gamma = \gamma - \gamma^*.$$

From the simplified yaw dynamics equations (9), and (10) and the motor model of (11), one can obtain

$$\ddot{e}_\gamma = -\frac{K_t}{I \cdot R_a} e_f + \frac{K_t^2}{I \cdot R_a}\dot{\psi} - \frac{1}{I} d_f, \tag{37}$$

where e_f is the control voltage and $I = I_{dz} + I_{bz} + I_{wz}$.

Let

$$e_f = -\frac{I \cdot R_a}{K_t}\left(v_f - \frac{K_t^2}{I \cdot R_a}\dot{\psi}\right). \tag{38}$$

It follows that

$$\ddot{e}_\gamma = v_f + d_3, \tag{39}$$

with $d_3 = -d_f/I$. Assume that d_3 is bounded and $|d_3| \leq \bar{d}_3$, where $\bar{d}_3$ is a known constant. The following sliding manifold is chosen

$$s_\gamma = \dot{e}_\gamma + \delta_\gamma e_\gamma = 0, \tag{40}$$

where $\delta_\gamma > 0$. As can be seen, in the manifold $s_\gamma = 0$, $e_\gamma \to 0$ as $t \to \infty$. Then, the following is chosen

$$v_f = -\delta_\gamma \dot{e}_\gamma - V_{o\gamma}\ \mathrm{sgn}(s_\gamma), \tag{41}$$

where $V_{o\gamma} > \bar{d}_3$ such that the reachability condition is satisfied. Finally, from (38) and (41), the control voltage is given by

$$e_f = -\frac{I \cdot R_a}{K_t}\left(-\delta_\gamma \dot{e}_\gamma - V_{o\gamma}\ \mathrm{sgn}(s_\gamma) - \frac{K_t^2}{I \cdot R_a}\dot{\psi}\right) \tag{42}$$

Once again, the $\mathrm{sgn}(\cdot)$ term in (42) is replaced by a saturation function in the implementation to eliminate the chattering problem.

V. POINT-TO-POINT MOTION CONTROL

In the previous section, the control schemes for maintaining balance and for regulating the position of the robot along a straight line from point to point were presented. Also, the control scheme for controlling the orientation of the robot as the robot maintains its upright position was designed. These control schemes can be used to obtain a simple form of point-to-point motion control. Consider the motion of the robot represented by a straight line segment with respect to the world frame $OXYZ$ shown in Fig. 3. Assuming that (x_0, y_0) are the coordinates of the initial contact point of the robot on the ground and γ_0 is the initial orientation of the robot with respect to the world frame, (x_1, y_1) are the coordinates of the end point of the motion and γ_1 is the desired orientation of the robot along the line segment. It is assumed that there is no slip in the wheel. As the robot moves from the initial point to the end point, the resulting angular displacement of the wheel is given by

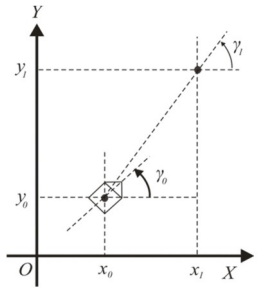

Fig. 3. Point-to-point motion control strategy.

$$\theta^* = \frac{\sqrt{(x_1 - x_0)^2 + (y_1 - y_0)^2}}{l_r}. \tag{43}$$

To balance the robot as it moves from the initial point to the end point along the desired line segment, the following strategy can be used:

1. Balance the robot at the initial point (x_0, y_0).
2. After balancing at (x_0, y_0), set the reference yaw angle to γ_1 and use the proposed steering control to rotate the robot about the point (x_0, y_0) from the initial yaw angle γ_0.
3. After the robot reaches the desire yaw angle, set the reference angle of the wheel to θ^* as given in (43) and regulate the robot in the straight line motion to the end point (x_1, y_1).

Since the orientation and translation of the robot are decoupled, the robot can easily rotate to the desired orientation after it has reached the goal point. For a path consisting of a sequence of line segments, by alternately regulating the position and rotating the orientation of the robot as described, the robot can follow the path to reach a specified goal.

VI. EXPERIMENTAL RESULTS

The designed control laws were implemented and tested on the experimental setup shown in Fig. 1. Two scenarios,

TABLE II
PARAMETERS OF EXPERIMENT

Moving in a Straight Line	(From $O \to A$)
Init. values (rad)	$\alpha = 0.0050$, $\beta = 0.010$, $\gamma = 0.5236$, others are set to zero.
Ref. angle of wheel (rad)	$\theta_A^* = 6$.
Ref. yaw angle (rad)	$\gamma_A^* = 0.5236$.
Length of line segment (m)	$l_{OA} = 0.3180$.
Moving to Multiple Points	(From $O \to A \to \ldots \to E \to O$)
Init. values (rad)	$\alpha = 0$, $\beta = 0$, $\gamma = 0$, others are set to zero.
Ref. angle of wheel (rad)	$\theta_A^* = 3$, $\theta_B^* = 6$, $\theta_C^* = 9$, $\theta_D^* = 12$, $\theta_E^* = 15$, $\theta_O^* = 18$.
Ref. yaw angle (rad)	$\gamma_A^* = 0$, $\gamma_B^* = 1.05$, $\gamma_C^* = 2.09$, $\gamma_D^* = 3.14$, $\gamma_E^* = 4.15$, $\gamma_O^* = 5.23$.
Length of line segments (m)	$l_{OA} = 0.16$, $l_{AB} = 0.16$, $l_{BC} = 0.16$, $l_{CD} = 0.16$, $l_{DE} = 0.16$, $l_{EO} = 0.16$.

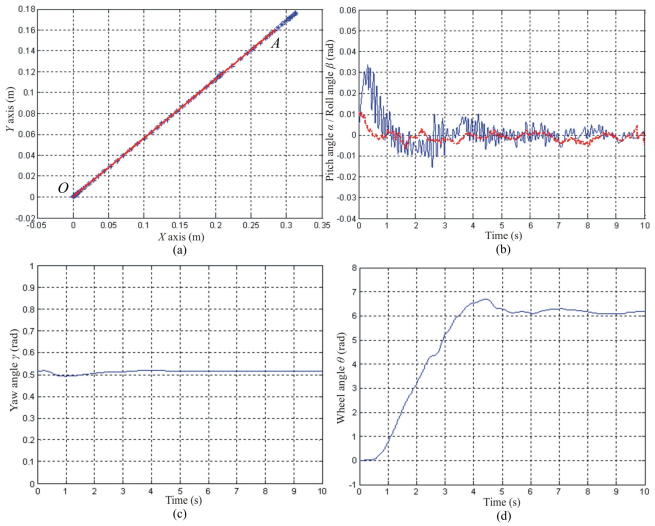

Fig. 4. Experimental results of moving along straight line: (a) *X-Y* trajectory (reference path: solid line, actual trajectory: star line), (b) pitch angle (solid line) and roll angle (dashdot line), (c) yaw angle, and (d) wheel angle.

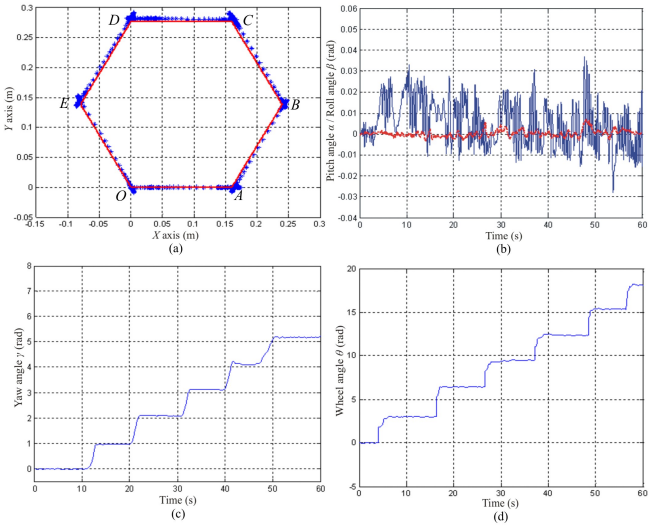

Fig. 5. Experimental results of moving to multiple waypoints: (a) *X-Y* trajectory (reference path: solid line, actual trajectory: star line), (b) pitch angle (solid line) and roll angle (dashdot line), (c) yaw angle, and (d) wheel angle.

namely (a) let the robot move along a straight line to reach a target, and (b) track a predefined path, are considered. The initial conditions of the system and the pre-defined reference paths given in Table II were used. The experimental results are shown in Figs. 4 and 5. Figures 4(a) and 5(a) show the trajectories of the robot in the world coordinates. The robot follows the reference path, moving from the initial point $O(0, 0)$ to the terminal point with a small deviation. The small deviation from the actual trajectory is possibly caused by unmodeled dynamics such as friction. As shown in the figures, the experimental results confirm that the robot maintains its balance as it moves and turns. A video clip demonstrating the performance of the robot is available at http://www.youtube.com/watch?v=PoG0H6yJp1Y. The experiment shows the feasibility of the designed control system.

VII. CONCLUDING REMARKS

The design, implementation, and validation of balance control and point-to-point motion control for a unicycle robot were presented. The mathematical model of the system was derived to facilitate the controller design. It has been shown that this system can be simplified to three decoupled systems. The control laws were then designed based on sliding mode control. The performance of the designed robotic system was validated and the experimental results show that the designed control schemes are capable of balancing and controlling the motion of the unicycle robot.

REFERENCES

[1] Y. Xu and Y. Ou, *Control of Single Wheel Robots*, Spinger, 2005.

[2] T. B. Lauwers, G. A. Kantor, and R. L. Hollis, "A dynamically stable single-wheeled mobile robot with inverse mouse-ball drive," in *Proc. of Int. Conf. on Robotics and Automation*, pp. 2884-2889, 2006.

[3] A. Schoonwinkel, *Design and Test of a Computer Stabilized Unicycle*, Ph.D. dissertation, Stanford Univ., Stanford, CA, 1987.

[4] D. W. Vos and A. H. von Flotow, "Dynamics and nonlinear adaptive control of an autonomous unicycle (theory and experiment)," in *Proc. 29th Conf. Decision Contr.*, pp.182-187, 1990.

[5] Z. Sheng and K. Yamafuji, "Postural stability of a human riding a unicycle and its emulation by a robot," *IEEE Trans. Robot. Autom.*, vol. 13, no. 5, pp. 709-720, 1997.

[6] Y. Naveh, P. Z. Bar-Yoseph, and Y. Halevi, "Nonlinear modeling and control of a unicycle," *Dynamics and Control*, Springer, vol. 9, no. 4, pp. 279-296, 1999.

[7] M. Q. Dao and K. Z. Liu, "Gain-scheduled stabilization control of a unicycle robot," *JSME Int. J.*, vol. 48, no. 4, pp.649-656, Jan. 2005.

[8] H. Jin, J. Hwang, and J. Lee, "A balancing control strategy for a one-wheel pendulum robot based on dynamic model decomposition: Simulations and experiments," *IEEE/ASME Trans on Mechatronics*, vol. 16, no. 4, pp. 763-768, Aug. 2011.

[9] J. Lee, S. Han, and J. Lee, "Decoupled dynamic control for pitch and roll axes of the unicycle robot," *IEEE Trans. on Industrial Electronics*, vol. 60, no. 9, pp. 3814-3822, Sep. 2013.

[10] Y. Fujimoto and S. Uchida, "Three dimensional posture control of mono-wheel robot with roll rotatable torso," in *Proc. IEEE Int. Conf. Mechatronics*, pp. 1-5, 2007.

[11] R. Nakajima, T. Tsubouchi, S. Yuta, and E. Koyanagi, "A development of a new mechanism of an autonomous unicycle," in *Proc. Int. Conf. on Intelligent Robots and Systems*, pp. 906-912, 1997.

[12] M. T. Ho, Y. Rizal, and Y. L. Chen, "Balance control of a unicycle robot," in *Proc. IEEE 23rd Int. Symposium on Industrial Electronics*, pp. 1186-1191, 2014.

[13] V. I. Utkin, *Sliding Modes in Control and Optimization*, B. W. Dickinson *et al.*, Eds. Berlin, Germany: Springer-Verlag, 1992.

[14] V. Utkin, J. Guldner, and J. Shi, *Sliding Mode Control in Electromechanical Systems*, Padstow, UK: Taylor & Francis, 1999.

[15] A. Isidori, *Nonlinear Control Systems*, Springer, London, 1995.

[16] J. H. Ginsberg, *Advanced Engineering Dynamics*, 2nd Ed, Cambridge, UK: Cambridge Univ. Press, 1998.

[17] ———, *Dynamics of a Unicycle System*, 2014. [Online]. Available: http://lab.es.ncku.edu.tw/csplab/appendixunicycle.pdf.

[18] Y. Kim, S. H. Kim, and Y. K. Kwak, "Dynamic analysis of a nonholonomic two-wheeled inverted pendulum robot," *J. Intelligent and Robotic Syst.*, vol. 44, no. 1, pp. 25-46, 2005.

[19] M. Spong, P. Corke, and R. Lozano, "Nonlinear control of the reaction wheel pendulum," *Automatica*, vol. 37, no. 11, pp. 1845-1851, 2001.

[20] S. V. Drakunov *et al.*, "The block control principle 1," *Automation and Remote Control*, vol. 51, no. 5, pp. 601-609, 1990.

[21] J. E. Slotine and W. Li, *Applied Nonlinear Control*, Englewood Cliffs, NJ: Prentice-Hall, 1991.